BULLETIN OF THE POLISH ACADEMY OF SCIENCES
TECHNICAL SCIENCES, Vol. 66, No. 4, 2018
DOI: 10.24425/124259

Fractional-order discrete model of an independent wheel electrical drive of the autonomous platform

M. BĄKAŁA*, J. NOWAKOWSKI, and P. OSTALCZYK

Institute of Applied Compute Science, Department of Electrical Engineering, Lodz University of Technology,
18/22 Stefanowskiego St., 90-924 Lodz, Poland

Abstract. In the paper the linear time-invariant fractional-order models of the separated wheel closed-loop electrical drive of the autonomous platform are considered. As a reference model one considers the classical model described by the second-order linear difference equation. Two discrete-time fractional-order models are considered: non-commensurate and commensurate. According to the sum of the squared error criterion (SSE) one compares two-parameter integer-order model with the four-parameter non-commensurate and three-parameter commensurate fractional-order ones. Three mathematical models are built and simulated. The computer simulation results are compared with measured velocity of the real autonomous platform separate wheel closed-loop electrical drive.

Key words: fractional-order backward-difference, difference equation, identification.

1. Introduction

The identification of real dynamical systems based on the fractional calculus mathematical tools [1–4] leads to better mathematical models [5–9] in the sense of a better matching of the data measured. Allowing any real orders in differential or difference equations provides a better fit due to the assumed criterion. On the other hand there is an increasing number of parameters to evaluate. In this paper non-commensurate vs. commensurate fractional-orders (FO) models are analyzed in terms of their effectiveness in modeling. The commensurate models are characterized by a smaller number of parameters. This is due to FOs set $\nu_p, \nu_{p-1}, \cdots, \nu_1$ in the non-commensurate system and $p\nu, (p-1)\nu, \cdots, \nu$ in the commensurate one. In both cases there is the same number of FODE coefficients. The paper contains a short introduction to the non-commensurate and commensurate systems described by linear FO difference equations and their state-space forms [10]. Then the closed-loop DC motor electrical drive of a separate wheel of an autonomous platform is described. Two simple linear models based on the FODEs are also proposed. The simulation results are compared with the measured data. The main conclusion of the analysis is the ability to achieve similar results in the identification with the two considered models. However, commensurate models have only one multiple order.

2. Non-commensurate and commensurate difference equation

Real dynamical systems modeling leads to mathematical models being differential equations

$$F\left[\frac{d^p y(t)}{dt^p}, \frac{d^{p-1} y(t)}{dt^{p-1}}, \cdots, \frac{y(t)}{dt}, y(t), \frac{d^q u(t)}{dt^q}, \frac{d^{q-1} u(t)}{dt^{q-1}}, \cdots, \frac{u(t)}{dt}, u(t), t\right] = 0, \tag{1}$$

where $y(t)$ and $u(t)$ denote the output and the input signals, respectively. Function F is in general non-linear. One can also admit fractional-order derivatives

$$F\left[{}_{t_0}^{GL}D_t^{\nu_p} y(t), {}_{t_0}^{GL}D_t^{\nu_{p-1}} y(t), \cdots, {}_{t_0}^{GL}D_t^{\nu_1} y(t), y(t), {}_{t_0}^{GL}D_t^{\mu_q} u(t), \cdots, {}_{t_0}^{GL}D_t^{\mu_1} u(t), u(t), t\right] = 0, \tag{2}$$

where ${}_{t_0}^{GL}D_t^{\nu} y(t)$ denotes the Grünwald-Letnikov fractional – order derivative

$${}_{t_0}^{GL}D_t^{(\nu)} f(t) = \lim_{h \to 0^+} \frac{{}_{k_0}^{GL}\Delta_k^{(\nu)} f(kh)}{h^\nu} \tag{3}$$

and all orders are arranged to satisfy inequalities $\nu_p > \nu_{p-1} > \cdots > \nu_1 > \nu_0 = 0, \mu_q > \mu_{q-1} > \cdots > \mu_1 > \mu_0 = 0$, $\nu_0 \neq \mu_0$ and all are rational numbers

$$\nu_i = \frac{e_i}{d_i} \quad \text{for} \quad i = 1, 2, \cdots, p, \quad \text{and} \quad e_i, d_i \in \mathbb{N}$$
$$\mu_j = \frac{g_j}{f_j} \quad \text{for} \quad j = 1, 2, \cdots, q, \quad \text{and} \quad g_j, f_j \in \mathbb{N} \tag{4}$$

and a finite sum for $\nu \in \mathbb{R}_+$

$${}_{k_0}^{GL}\Delta_k^{(\nu)} f(k) = \sum_{i=k_0}^{k} a^{(\nu)}(i-k_0) f(k+k_0-i) = \sum_{i=0}^{k-k_0} a^{(\nu)}(i) f(k-i), \tag{5}$$

denotes the Grüwald-Letnikov fractional-order backward difference (GL-FOBD). Moreover,

*e-mail: mbakala@kis.p.lodz.pl

Manuscript submitted 2018-03-07, revised 2018-05-16, 2018-06-19, and 2018-07-23, initially accepted for publication 2018-08-14, published in August 2018.

$$a^{(\nu)}(k)=\begin{cases}0 & \text{for} \quad k<0\\ 1 & \text{for} \quad k=0\\ (-1)^k\frac{\nu(\nu-1)\cdots(\nu-k+1)}{k!} & \text{for} \quad k=1,2,3,\cdots\end{cases} \tag{6}$$

The GL-FOBD divided by a finite sampling time h (which should be relatively small) in (2) approximates the derivatives

$$\begin{aligned}{}_{t_0}^{GL}D_t^{(\nu_i)}y(t)&\approx\frac{{}_{k_0h}^{GL}\Delta_{kh}^{(\nu_i)}y(kh)}{h^{\nu_i}},\\ {}_{t_0}^{GL}D_t^{(\mu_j)}u(t)&\approx\frac{{}_{k_0h}^{GL}\Delta_{kh}^{(\mu_j)}u(kh)}{h^{\mu_j}}.\end{aligned} \tag{7}$$

Hence, for $i=1,2,\cdots,p$, $j=1,2,\cdots,q$ from (2) one obtains the FO difference equation (FODE)

$$\begin{aligned}&F\left[{}_{k_0h}^{GL}\Delta_{kh}^{(\nu_p)}y(kh),\cdots,{}_{k_0h}^{GL}\Delta_{kh}^{(\nu_1)}y(kh),y(kh),\right.\\ &\left.{}_{k_0h}^{GL}\Delta_{kh}^{(\mu_q)}u(kh),\cdots,{}_{k_0h}^{GL}\Delta_{kh}^{(\mu_1)}u(kh),u(kh),kh\right]=0.\end{aligned} \tag{8}$$

Let d be the least common denominator of fractions (4). Then, the orders take the forms

$$\nu_i=n_i\nu \quad \text{for} \quad i=1,2,\cdots,p, \quad \text{and} \quad n_i,d\in\mathbb{N} \tag{9}$$

$$\mu_j=m_j\nu \quad \text{for} \quad j=1,2,\cdots,q, \quad \text{and} \quad m_j,d\in\mathbb{N} \tag{10}$$

where

$$\nu=\frac{1}{d}. \tag{11}$$

Then, introducing the notation given above, the considered FOBDs can be expressed in a form

$$\begin{aligned}{}_{k_0h}^{GL}\Delta_{kh}^{(\nu_i)}y(kh)&={}_{k_0h}^{GL}\Delta_{kh}^{(n_i\nu)}y(kh)\\ &=\left[\underbrace{{}_{k_0h}^{GL}\Delta_{kh}^{(\nu)}{}_{k_0h}^{GL}\Delta_{kh}^{(\nu)}\cdots{}_{k_0h}^{GL}\Delta_{kh}^{(\nu)}}_{n_i}\right]y(kh)\end{aligned} \tag{12}$$

and

$$\begin{aligned}{}_{k_0h}^{GL}\Delta_{kh}^{(\mu_i)}u(kh)&={}_{k_0h}^{GL}\Delta_{kh}^{(m_i\mu)}u(kh)\\ &=\left[\underbrace{{}_{k_0h}^{GL}\Delta_{kh}^{(\mu)}{}_{k_0h}^{GL}\Delta_{kh}^{(\mu)}\cdots{}_{k_0h}^{GL}\Delta_{kh}^{(\mu)}}_{m_i}\right]u(kh)\end{aligned} \tag{13}$$

Under the above forms the FODE (8) takes the form

$$\begin{aligned}&F\left[{}_{k_0h}^{GL}\Delta_{kh}^{(n_p\nu)}y(kh),\cdots,{}_{k_0h}^{GL}\Delta_{kh}^{(n_1\nu)}y(kh),y(kh),\right.\\ &\left.{}_{k_0h}^{GL}\Delta_{kh}^{(m_q\nu)}u(kh),\cdots,{}_{k_0h}^{GL}\Delta_{kh}^{(m_1\nu)}u(kh),u(kh),kh\right]=0.\end{aligned} \tag{14}$$

for $p>q\in\mathbb{N}$ and $n_p>m_q$.

Assuming that for an input signal having the property

$$\lim_{k\to+\infty}u(kh)=u_s=\text{const} \tag{15}$$

there exists a steady-state solution of (8) and (14)

$$\lim_{k\to+\infty}y(kh)=y_s=\text{const}. \tag{16}$$

It means that the algebraic equation

$$F\left[0,\cdots,0,y_s,0,0,\cdots,0,u_s,0\right]=0 \tag{17}$$

is satisfied. The linearization procedure is described in details in [10].

2.1. Non-commensurate and commensurate linear time-invariant FODE. A special but very important class of the FOBDs is a class of stable linear time-invariant FOBD [11, 12]. For the non-linear FODEs one can apply the linearization procedure around the steady-state conditions and under the assumption of a relatively small change of the input signal. This is the first approach in the system modeling. To simplify a notation further on we transform a discrete-time scale to assume $h=1$. The linear time invariant non-commensurate FODE is of the form

$$\sum_{i=0}^{p}a_i{}_{k_0}^{GL}\Delta_k^{(\nu_i)}y(k)=\sum_{j=0}^{q}b_j{}_{k_0}^{GL}\Delta_k^{(\nu_j)}u(k)=\widehat{u}(k), \tag{18}$$

where the FOs are ordered in the same way as in (2). The linear time-invariant commensurate FODE is as follows

$$\sum_{i=0}^{p}a_i{}_{k_0}^{GL}\Delta_k^{(n_i\nu)}y(k)=\sum_{j=0}^{q}b_j{}_{k_0}^{GL}\Delta_k^{(m_j\nu)}u(k)=\widehat{u}(k), \tag{19}$$

with a_i, b_j and $a_p=1$ are constant coefficients, $p\geq q$ and $u(k)$ is a known input signal. For $d=1$ in (19) i.e. $\nu=1$ the considered FOBD represents the classical integer – order difference equations (IOBD).

Proposition 1. Every rational-order non-commensurate system can be transformed to the commensurate one.

The proof and transformation procedure is described in [10].

2.2. State-space equations of the non-commensurate and commensurate systems. The FOBD has a concatenation property

$${}_{k_0}^{GL}\Delta_k^{(\nu)}\left[{}_{k_0}^{GL}\Delta_k^{(\mu)}y(k)\right]={}_{k_0}^{GL}\Delta_k^{(\nu+\mu)}y(k), \tag{20}$$

for $\nu,\mu\geq 0$.

Now we present a splitting algorithm transforming given real numbers set ν_i, $i=1,2,\cdots,p$ and μ_j, $j=1,2,\cdots,q$ into a set of sums of lower numbers. Denote $s=p+q$ and

$$\mathbf{S}=\{\nu_p,\nu_{p-1},\cdots,\nu_1,\mu_q,\mu_{q-1},\cdots,\mu_1\}. \tag{21}$$

The set's (21) elements are inserted in Table 1.

Table 1
Step 0

$\cdots$	$\{\rho_{0,4}\}$	$\{\rho_{0,3}\}$	$\{\rho_{0,2}\}$	$\{\rho_{0,1}\}$

In the Step 1 all elements but the last one are represented as a sum

$$\rho_{0,i}=\rho_{1,i}+\rho_{0,1} \quad \text{for} \quad i=p+q,p+q-1,\cdots,2. \tag{22}$$

Hence, every elementent is represented by two numbers $\{\rho_{1,i}\{\rho_{0,1}\}\}$ for $i=p+q,p+q-1,\cdots,2$. These two components represent an element in the same column and above row. Both Steps are represented in Table 2.

Table 2
Step 1

$\cdots$	$\{\rho_{0,4}\}$	$\{\rho_{0,3}\}$	$\{\rho_{0,2}\}$	$\{\rho_{0,1}\}$
$\cdots$	$\{\rho_{1,4},\{\rho_{0,1}\}\}$	$\{\rho_{1,3},\{\rho_{0,1}\}\}$	$\{\rho_{1,2},\{\rho_{0,1}\}\}$	$\{\rho_{0,1}\}$

In the Step 2 all elements but the two last are represented as a sum

$$\rho_{0,i} = \rho_{2,i} + \rho_{1,2} + \rho_{0,1} \text{ for } i = p, p-1, \cdots, 3 \tag{23}$$

After this operation we get a Table 3.

Table 3
Step 2

$\cdots$	$\{\rho_{0,4}\}$	$\{\rho_{0,3}\}$	$\{\rho_{0,2}\}$	$\{\rho_{0,1}\}$
$\cdots$	$\{\rho_{1,4},\{\rho_{0,1}\}\}$	$\{\rho_{1,3},\{\rho_{0,1}\}\}$	$\{\rho_{1,2},\{\rho_{0,1}\}\}$	$\{\rho_{0,1}\}$
$\cdots$	$\{\rho_{2,4},\{\rho_{2,2},\rho_{0,1}\}\}$	$\{\rho_{2,3},\{\rho_{2,2},\rho_{0,1}\}\}$	$\{\rho_{2,2},\{\rho_{0,1}\}\}$	$\{\rho_{0,1}\}$
$\cdots$	$\vdots$	$\vdots$	$\vdots$	$\vdots$

The Algorithm will be illustrated in a numerical example.

2.2.1. Numerical example. For a set of orders

$$\mathbf{S} = \{0.8, 0.5, 0.3, 0.1\} \tag{24}$$

we get the following Table 4.

Table 4
Table of numerical example

{0.8}	{0.5}	{0.3}	{0.1}
{ 0.7, {0.1}}	{ 0.4, {0.1}}	{ 0.2, {0.1}}	{ 0.1 }
{ 0.5, {0.2,0.1}}	{ 0.2, {0.2,0.1}}	{ 0.2,{0.1}}	{0.1 }
{0.3,{ 0.2,0.2,0.1}}	{ 0.2, {0.2,0.1}}	{ 0.2,{0.1}}	{0.1 }

Remark 1. One should realize that elements representing the sum of cells in a chosen column are equal

$$\rho_{0,k} = \sum_{i=2}^{k} \rho_{l,i} + \rho_{0,1} \quad \text{for} \quad l = 1, 2, \cdots, l_{\max}, \tag{25}$$

where $l_{\max}$ denotes the last row when the elements cannot be splitted further.

Remark 2. One should reassign elements $\rho_{0,i}$ to appropriate orders ν_j and μ_k.

Then, in view of equality (25) appropriate FOBD are represented as products of FOBDs

$${}_{k_0}^{GL}\Delta_k^{(\nu_i)} y(k) = \prod_{j=2}^{i} {}_{k_0}^{GL}\Delta_k^{(\rho_{l_{\max},i})} {}_{k_0}^{GL}\Delta_k^{(\rho_{0,1})} y(k). \tag{26}$$

Applying (26), FODE may be expressed in a form

$$\begin{aligned} &\sum_{i=0}^{p} a_i \prod_{j=2}^{i} {}_{k_0}^{GL}\Delta_k^{(\rho_{l_{\max},i})} {}_{k_0}^{GL}\Delta_k^{(\rho_{0,1})} y(k) \\ &= \sum_{i=0}^{q} b_i \prod_{j=2}^{i} {}_{k_0}^{GL}\Delta_k^{(\rho_{l_{\max},i})} {}_{k_0}^{GL}\Delta_k^{(\rho_{0,1})} u(k). \end{aligned} \tag{27}$$

Remark 3. To avoid too many indices in (27) an equivalent notation is introduced

$$\nu_i = \sum_{s=1}^{i} \widehat{\nu}_s, \qquad \mu_j = \sum_{t=1}^{j} \widehat{\nu}_t. \tag{28}$$

Then, equation (27) takes a form

$$\begin{aligned} &\sum_{i=0}^{p} a_i {}_{k_0}^{GL}\Delta^{(\widehat{\nu}_i)} \cdots {}_{k_0}^{GL}\Delta_k^{(\widehat{\nu}_i)} y(k) \\ &= \sum_{i=0}^{q} a_i {}_{k_0}^{GL}\Delta^{(\widehat{\nu}_i)} \cdots {}_{k_0}^{GL}\Delta_k^{(\widehat{\nu}_i)} u(k). \end{aligned} \tag{29}$$

Now, we define new variables called further state-variables

$$\begin{aligned} y(k) &= x_1(k) \\ {}_{k_0}^{GL}\Delta_k^{(\widehat{\nu}_1)} y(k) &= {}_{k_0}^{GL}\Delta_k^{(\widehat{\nu}_1)} x_1(k) = x_2(k) \\ {}_{k_0}^{GL}\Delta_k^{(\widehat{\nu}_2)} \left[{}_{k_0}^{GL}\Delta_k^{(\widehat{\nu}_1)} y(k) \right] &= {}_{k_0}^{GL}\Delta_k^{(\widehat{\nu}_2)} x_2(k) = x_3(k) \\ &\vdots \\ {}_{k_0}^{GL}\Delta_k^{(\widehat{\nu}_{p-1})} x_{p-1}(k) &= x_p(k) \end{aligned} \tag{30}$$

A substitution of the elements of the above set of state-variables into (30) gives

$${}_{k_0}^{GL}\Delta_k^{(\widehat{\nu}_p)} x_p(k) = -\sum_{i=1}^{p-1} a_i x_i(k) + u(k). \tag{31}$$

Equations (30) and (31) can be expressed in the matrix-vector form

$${}_{k_0}^{GL}\Delta_k^{(\boldsymbol{\nu})} \mathbf{x}(k) = \mathbf{A}\mathbf{x}(k) + \mathbf{b}u(k), \tag{32}$$

$$y(k) = \mathbf{c}\mathbf{x}(k) + \mathbf{b}u(k), \tag{33}$$

where

$${}_{k_0}^{GL}\Delta_k^{(\boldsymbol{\nu})} \mathbf{x}(k) = \begin{bmatrix} {}_{k_0}^{GL}\Delta_k^{(\widehat{\nu}_1)} x_1(k) \\ {}_{k_0}^{GL}\Delta_k^{(\widehat{\nu}_2)} x_2(k) \\ \vdots \\ {}_{k_0}^{GL}\Delta_k^{(\widehat{\nu}_{p-1})} x_{p-1}(k) \\ {}_{k_0}^{GL}\Delta_k^{(\widehat{\nu}_p)} x_p(k) \end{bmatrix}, \tag{34}$$

$$\boldsymbol{\nu} = \begin{bmatrix} \widehat{\nu}_1 \\ \widehat{\nu}_2 \\ \vdots \\ \widehat{\nu}_{p-1} \\ \widehat{\nu}_p \end{bmatrix}, \qquad \mathbf{x}(k) = \begin{bmatrix} x_1(k) \\ x_2(k) \\ \vdots \\ x_{p-1}(k) \\ x_p(k) \end{bmatrix}, \tag{35}$$

$$\mathbf{A} = \begin{bmatrix} 0 & 1 & 0 & \cdots & 0 & 0 \\ 0 & 0 & 1 & \cdots & 0 & 0 \\ \vdots & \vdots & \vdots & & \vdots & \vdots \\ 0 & 0 & 0 & \cdots & 0 & 1 \\ -a_0 & -a_1 & -a_2 & \cdots & -a_{p-2} & -a_{p-1} \end{bmatrix}, \quad \mathbf{b} = \begin{bmatrix} 0 \\ 0 \\ \vdots \\ 0 \\ 1 \end{bmatrix}, \tag{36}$$

$$\mathbf{c} = \begin{bmatrix} b_0 & b_1 & \cdots & b_q & 0 & \cdots & 0 \end{bmatrix}, \quad \mathbf{d} = [1]. \tag{37}$$

In the case of the commensurate system $\widehat{\nu}_i = i\nu$ for $i = 1, 2, \cdots, p$. Hence, the left-hand side vector (35) simplifies essentially

$$ {}_{k_0}^{GL}\Delta_k^{(\nu)}\mathbf{x}(k) = \begin{bmatrix} {}_{k_0}^{GL}\Delta_k^{(\nu)}x_1(k) \\ {}_{k_0}^{GL}\Delta_k^{(\nu)}x_2(k) \\ \vdots \\ {}_{k_0}^{GL}\Delta_k^{(\nu)}x_{p-1}(k) \\ {}_{k_0}^{GL}\Delta_k^{(\nu)}x_p(k) \end{bmatrix} = {}_{k_0}^{GL}\Delta_k^{(\nu)} \begin{bmatrix} x_1(k) \\ x_2(k) \\ x_3(k) \\ \vdots \\ x_{p-1}(k) \\ x_p(k) \end{bmatrix}. \quad (38) $$

Classical ARX [13] models are described by linear difference equation

$$ \sum_{i=0}^{p} c_{p-i}y(kh - ih) = \sum_{i=0}^{q} d_{q-i}u(kh - ih) + n(kh) \quad (39) $$

with $c_p = 1$ and $n(kh)$ denoting a white-noise signal. The following Proposition shows that the ARX model can be equivalently described by a linear difference equation.

Proposition 2. The ARX model described by equation (41) has an equivalent representation

$$ \sum_{i=0}^{p} C_{p-i}{}_{p-i}^{GL}\Delta_k^{(i)}y(kh) = \sum_{i=0}^{q} D_i{}_{k-i}^{GL}\Delta_k^{(i)}u(kh) + n(kh). \quad (40) $$

Proof. Equation (41) can be equivalently described in a vector form

$$ \begin{aligned} &\begin{bmatrix} 1 & c_{p-1} & c_{p-2} & \cdots & c_1 & c_0 \end{bmatrix} \begin{bmatrix} y(k) \\ y(k-1) \\ \vdots \\ y(k-p+1) \\ y(k-p) \end{bmatrix} \\ &= \begin{bmatrix} d_q & d_{q-1} & d_{q-2} & \cdots & d_1 & d_0 \end{bmatrix} \begin{bmatrix} u(k) \\ u(k-1) \\ \vdots \\ u(k-q+1) \\ u(k-q) \end{bmatrix} + n(k) \end{aligned} \quad (41) $$

Now we define a matrix

$$ \mathbf{T}_{p+1} = \begin{bmatrix} a^{(p)}(0) & a^{(p)}(1) & \cdots & a^{(p)}(p-1) & a^{(p)}(p) \\ a^{(p-1)}(0) & a^{(p-1)}(1) & \cdots & a^{(p-1)}(p-1) & 0 \\ \vdots & \vdots & & \vdots & \vdots \\ a^{(1)}(0) & a^{(1)}(1) & \cdots & 0 & 0 \\ a^{(0)}(0) & 0 & \cdots & 0 & 0 \end{bmatrix}. \quad (42) $$

Its inverse can be easily calculated

$$ \mathbf{T}_{p+1}^{-1} = \begin{bmatrix} 0 & 0 & \cdots & 0 & a^{(0)}(0) \\ 0 & 0 & \cdots & a^{(1)}(1) & a^{(1)}(0) \\ \vdots & \vdots & & \vdots & \vdots \\ 0 & a^{(p-1)}(p-1) & \cdots & a^{(p-1)}(1) & a^{(p-1)}(0) \\ a^{(p)}(p) & a^{(p)}(p-1) & \cdots & a^{(p)}(1) & a^{(p)}(0) \end{bmatrix}. \quad (43) $$

Next we express equation (43) as

$$ \begin{aligned} &\begin{bmatrix} 1 & c_{p-1} & \cdots & c_1 & c_0 \end{bmatrix} \mathbf{T}_{p+1}^{-1}\mathbf{T}_{p+1} \begin{bmatrix} y(k) \\ y(k-1) \\ \vdots \\ y(k-p+1) \\ y(k-p) \end{bmatrix} \\ &= \begin{bmatrix} 1 & d_{q-1} & \cdots & d_1 & d_0 \end{bmatrix} \mathbf{T}_{q+1}^{-1}\mathbf{T}_{q+1} \begin{bmatrix} u(k) \\ u(k-1) \\ \vdots \\ u(k-q+1) \\ u(k-q) \end{bmatrix} + n(k). \end{aligned} \quad (44) $$

Then, we get

$$ \begin{aligned} &\begin{bmatrix} C_p & C_{p-1} & \cdots & C_1 & C_0 \end{bmatrix} \begin{bmatrix} {}_{k-p}^{GL}\Delta_k^{(p)}y(k) \\ {}_{k-p-1}^{GL}\Delta_k^{(p-1)}y(k) \\ \vdots \\ {}_{k-1}^{GL}\Delta_k^{(1)}y(k) \\ y(k) \end{bmatrix} \\ &= \begin{bmatrix} D_p & \cdots & D_1 & D_0 \end{bmatrix} \begin{bmatrix} {}_{k-q}^{GL}\Delta_k^{(q)}u(k) \\ {}_{k-q-1}^{GL}\Delta_k^{(q-1)}u(k-1) \\ {}_{k-q-2}^{GL}\Delta_k^{(q-2)}y(k)u(k-2) \\ \vdots \\ {}_{k-1}^{GL}\Delta_k^{(1)}y(k)u(1) \\ u(k) \end{bmatrix} + n(k), \end{aligned} \quad (45) $$

where

$$ \begin{aligned} C_j &= \sum_{i=0}^{p-j} c_i a^{(p-i)}(j) \quad \text{for} \quad j = 0, 1, \cdots, p, \\ D_j &= \sum_{i=0}^{q-j} d_i a^{(q-i)}(j) \quad \text{for} \quad j = 0, 1, \cdots, q. \end{aligned} \quad (46) $$

□

3. Separated-wheel closed-loop DC motor electrical drive description

The 6-wheeled autonomous platform with 6 independent closed-loop DC motor drives with 6 identical PI controllers is considered. It is presented in Fig. 1. Figure 4 presents a new

measuring stand, which was designed and manufactured. It consists of the extortion plate (1), sensors of displacement (2) and the holder of the aluminum frame (3). The measurement is based on determining with certain frequency and amplitude the movement of the swing arm excited by a force plate. After obtaining a fixed plate movement, it was switched off. The movement of the swing arm was measured by displacement sensors. The results from the experiments carried out for different settings were recorded in real time.

Fig. 1. Photo of the 6-wheel autonomous platform

The block diagram of a closed-loop system [14, 15] of one separated DC drive block diagram [16, 17] electrical drive [18] is given in Fig. 2.

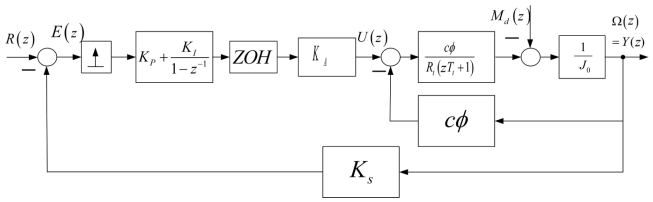

where the $\mathcal{Z}$-Transforms [19] denote:

- $R(z)$ – the $\mathcal{Z}$-Transform of a reference signal,
- $E(z)$ – the $\mathcal{Z}$-Transform of an error signal,
- $U(z)$ – the $\mathcal{Z}$-Transform of an controlling signal,
- $Y(z)$ – the $\mathcal{Z}$-Transform of the angular velocity of a motor wheel,
- $M_d(z)$ – the $\mathcal{Z}$-Transform of an external disturbance moment representing resistive moment due to rolling resistance,
- R_t – the motor's armature resistance,
- $T_t = \frac{L_t}{R_t}$ – a time constant, where L_t denotes the armature's inductance,
- $c\Phi$ – the motor constant,
- J_o – combined mass moment of inertia of the flywheel and shaft and armature,
- K_P – the PI controller proportional part gain,
- K_I – the PI controller integration part gain,
- K_S – the sensor gain,
- K_A – the amplifier gain.

Fig. 2. Block diagram of the closed-loop DC motor drive of the separated platform wheel

The DC motor and the PI controller are described by difference equations

$$\begin{aligned} {}^{GL}_{k-2}\Delta^{(2)}_k u(kh) + a_1 {}^{GL}_{k-1}\Delta^{(1)}_k u(kh) + a_0 u(kh) \\ = b_1 u(kh-h), \end{aligned} \tag{47}$$

$$u(kh) = K_P e(kh) + K_{I0} {}^{GL}\Delta^{(-1)}_k e(kh).$$

Combining equations presented above with an adder $e(kh) = r(kh) - K_S\omega(kh)$ we get the difference equation describing the ARX model [13] transformed according to (40). The PI controller parameters are tuned to get a quick start preserving bounded signal values (maximal current and control voltage). Two models are evaluated: an integer and a fractional one. The model parameters are given in Table 5.

Table 5
6-wheel autonomous platform measured and simulated models responses

Model	a_3	a_2	a_1	b_2	b_1	b_0	ν	μ
(18)	0.9127	8.49e-2	2.1e-3	3e-4	1.21	-3.6317	3,2,1,0	2,1,0
(19)	–	–	1	24.28	24.28	–	1.16	0

The velocity of the platform on a flat and hard surface is presented in Fig. 3. The sum of squared errors (SSE) criteria are equal. The integer model has 6 parameters whereas fractional one only 3. This is an advantage of a fractional model.

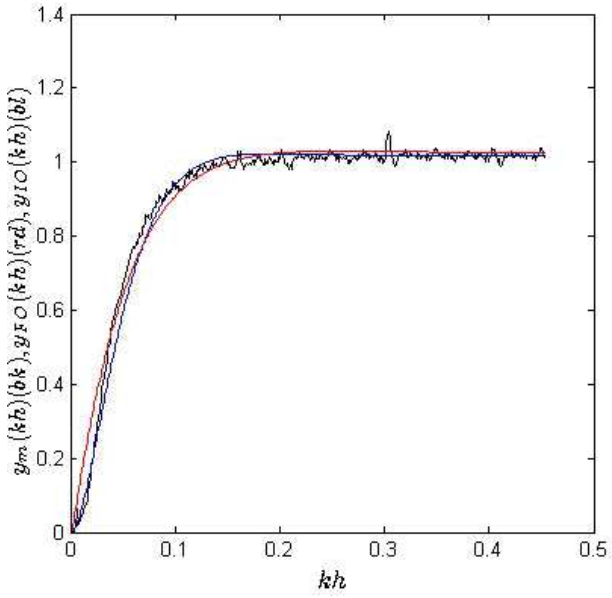

Fig. 3. Normalized step response of a 6-wheel autonomous platform (black) and integer (blue) and fractional (red) models responses

3.1. DC motor-drive of a separated wheel. When the platform corps is suspended, the main wheel rolling resistance is almost zero. Then, the step response of the separated wheel is characterized by a huge overshoot. The settings of regulator parameters are the same. The separated wheel photo, its model and a measured angular velocity are presented in Figs. 4–6, respectively.

Fig. 4. Autonomous platform wheel photo

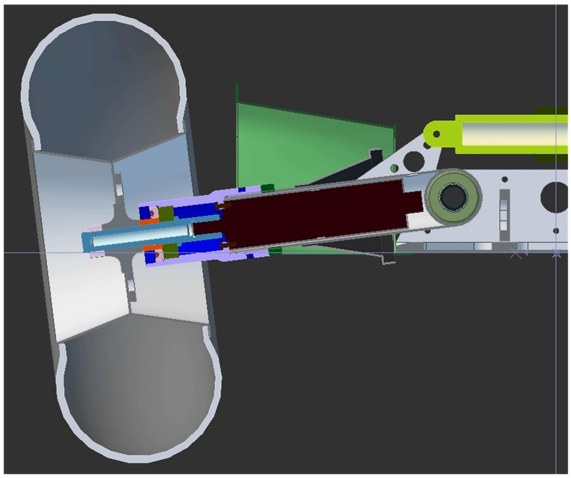

Fig. 5. Autonomous platform wheel model 2D view-3

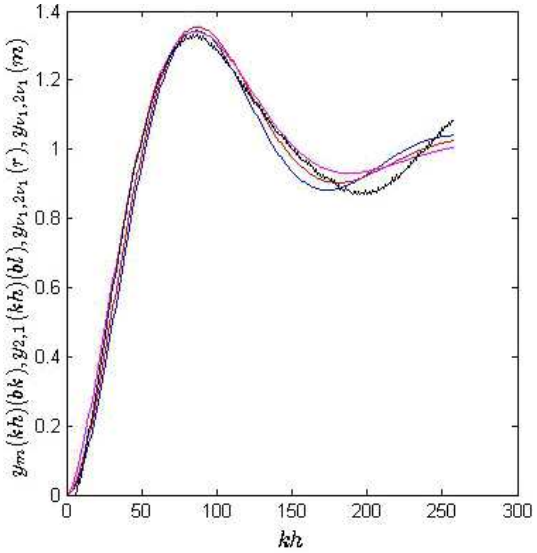

Fig. 6. Step response of a separated wheel with simulated responses

To simplify the identification of the electrical DC drive notation we perform a time-scale transformation to get $h = 1$. Further on, the numerical step $h = 1$ will be omitted. It is a bijection transformation to original time scale.

Table 6
Model parameters

Model	a_1	a_0	ν_1	ν_2	SSE
(48)	0.1447	0.01447	1	2	0.1588
(50)	0.145	0.01460	1.1	1.9	0.070511
(52)	0.144	0.01456	0.8	1.6	0.071735

3.1.1. Measured transient characteristics. In the experiment there was assumed a reference signal $d(k) = 0$ and an external disturbance moment $m_d(k) = \text{const} < 0$ in a shape of the discrete-step function. Presented in Fig. 7 discrete step response suggests the second order damped oscillation models. Evidently, in the "black box" measured data there are hidden non-linear frictions and external disturbance moments which the non-commensurate and commensurate FODE models should describe.

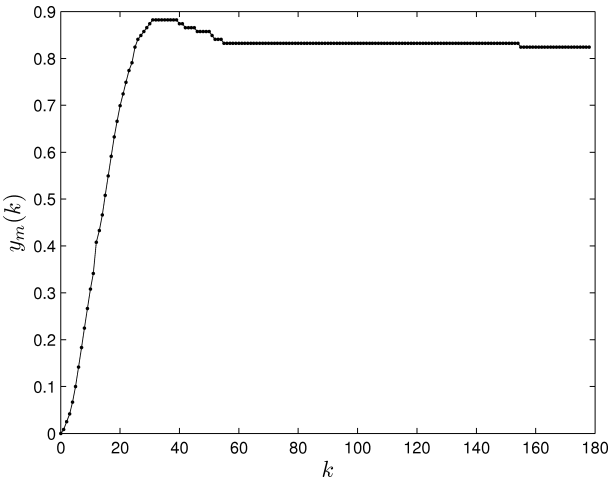

Fig. 7. Measured wheel-drive system step response

3.2. Classical two-parameter linear integer-orders difference equation model of the wheel-drive. As the mentioned classical oscillation model one takes (18) with $p = 2, q = 0$, $\nu_2 = 2, \nu_1 = 1$. The assumption means that the stable model [20, 21] is described by the IODE of the form

$$\begin{aligned} {}_{k_0}^{GL}\Delta_k^{(2)} y_{1,2}(k) + a_1 {}_{k_0}^{GL}\Delta_k^{(1)} y_{1,2}(k) + a_0 y_{1,2}(k) \\ = a_0 m_d(k), \end{aligned} \tag{48}$$

where $y_{1,2}$ is an angle of classical integer model. Without prejudice to the generality of considerations one can assume $b_0 = a_0$. Hence, one gets the two-parameter model a_1, a_0. The integer orders are 2 and 1. The related state-space form is as follows

$$\begin{aligned} {}_{k_0}^{GL}\Delta_k^{(1)} \begin{bmatrix} x_1(k) \\ x_2(k) \end{bmatrix} &= \begin{bmatrix} 0 & 1 \\ -a_0 & -a_1 \end{bmatrix} + \begin{bmatrix} 0 \\ 1 \end{bmatrix} m_d(k), \\ y_{1,2}(k) &= \begin{bmatrix} 1 & 0 \end{bmatrix} \begin{bmatrix} x_1(k) \\ x_2(k) \end{bmatrix} + [a_0]\, m_d(k). \end{aligned} \tag{49}$$

3.3. Non-commensurate three-parameter linear fractional-order difference equation model of the wheel-drive. As a special case of (18) one assumes the four-parameter model

$$ {}_{k_0}^{GL}\Delta_k^{(\nu_2)} y_{\nu_1,\nu_2}(k) + a_1 {}_{k_0}^{GL}\Delta_k^{(\nu_1)} y_{\nu_1,\nu_2}(k) + a_0 y_{\nu_1,\nu_2}(k) = a_0 m_d(k). \tag{50} $$

Related state-space equations are

$$ \begin{bmatrix} {}_{k_0}^{GL}\Delta_k^{(\nu_1)} x_1(k) \\ {}_{k_0}^{GL}\Delta_k^{(\nu_2-\nu_1)} x_2(k) \end{bmatrix} = \begin{bmatrix} 0 & 1 \\ -a_0 & -a_1 \end{bmatrix} + \begin{bmatrix} 0 \\ 1 \end{bmatrix} m_d(k), $$
$$ y_{\nu_1,\nu_2}(k) = \begin{bmatrix} 1 & 0 \end{bmatrix} \begin{bmatrix} x_1(k) \\ x_2(k) \end{bmatrix} + [a_0]\, m_d(k) \tag{51} $$

with unknown four parameters a_1, a_0, ν_2, ν_1.

3.4. Commensurate linear fractional-order state-space model of the wheel-drive. The FODE has three parameters: a_1, a_0 and $\nu \in \mathbb{R}_+$

$$ {}_{k_0}^{GL}\Delta_k^{(2\nu)} y_{\nu,2\nu}(k) + a_1 {}_{k_0}^{GL}\Delta_k^{(\nu)} y_{\nu,2\nu}(k) + a_0 y_{\nu,2\nu}(k) = a_0 m_d(k), \tag{52} $$

$$ {}_{k_0}^{GL}\Delta_k^{(\nu)} \begin{bmatrix} x_1(k) \\ x_2(k) \end{bmatrix} = \begin{bmatrix} 0 & 1 \\ -a_0 & -a_1 \end{bmatrix} + \begin{bmatrix} 0 \\ 1 \end{bmatrix} r(k), $$
$$ y_{\nu,2\nu}(k) = \begin{bmatrix} 1 & 0 \end{bmatrix} \begin{bmatrix} x_1(k) \\ x_2(k) \end{bmatrix} + [a_0]\, m_d(k). \tag{53} $$

4. Comparison of models

An optimal choice of parameters related to three linear structures described by formulas (48), (50) and (52) is based on the minimization of a performance index SSE. Denoting the measured output signal as $y_m(k)$ one defines three error functions

$$ e_{1,2}(k) = y_m(k) - y_{1,2}(k), \tag{54} $$
$$ e_{\nu_1,2\nu_1}(k) = y_m(k) - y_{\nu_1,2\nu_1}(k) \tag{55} $$
$$ e_{\nu_1,\nu_2}(k) = y_m(k) - y_{\nu_1,\nu_2}(k) \tag{56} $$

then the criteria are the functions as follows

$$ \mathrm{SSE}(a_0, a_1) = \sum_{k=0}^{k_{\max}} e_{1,2}^2(k), \tag{57} $$

$$ \mathrm{SSE}(a_0, a_1, \nu_1, \nu_2) = \sum_{k=0}^{k_{\max}} e_{\nu_1,\nu_2}^2(k), \tag{58} $$

$$ \mathrm{SSE}(a_0, a_1, \nu_1) = \sum_{k=0}^{k_{\max}} e_{\nu_1,2\nu_1}^2(k). \tag{59} $$

Numerically found minimal values of coefficients and FOs are collected in Table 7.

Table 7
Identification effects comparison

Model	a_1	a_0	ν_1	ν_2	SSE
(48)	0.1447	0.01447	1	2	0.0360
(50)	0.145	0.01460	0.993	1.931	0.0175
(52)	0.144	0.01456	0.983	1.966	0.0249

The plots of measured output signal $y_m(kh)$ and simulated responses $y_{2,1}$, y_{ν_1,ν_2}, $y_{\nu_1,2\nu_1}$ are presented in Fig. 8. Figure 9 shows enlarged fragment of Fig. 8.

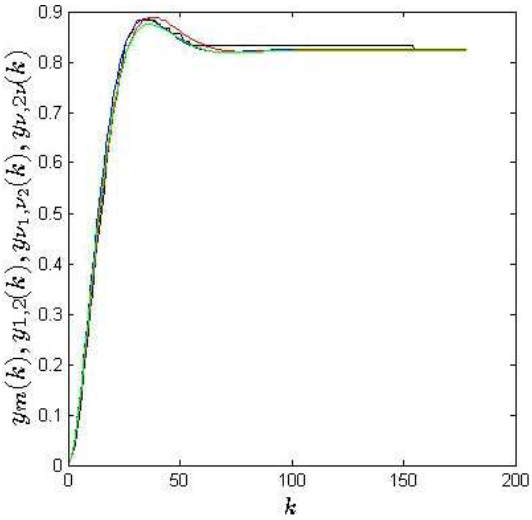

Fig. 8. Plots of measured $y_m(k)$ (black), simulated IO response $y_{1,2}(k)$ (blue) and FO models responses: non-commensurate $y_{\nu_1,\nu_2}(k)$ (red) and commensurate $y_{\nu,2\nu}(k)$ (green)

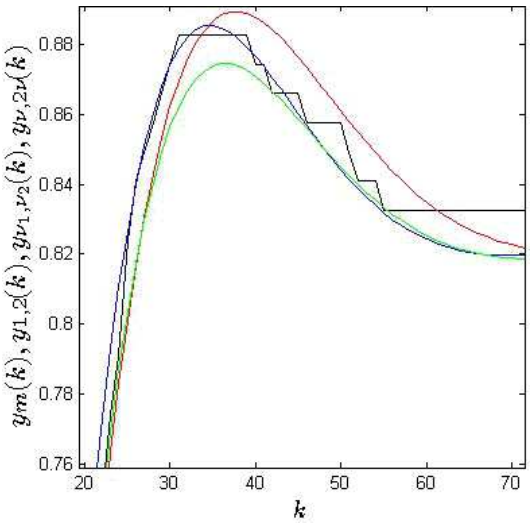

Fig. 9. Enlarged fragment of Fig. 8

5. Conclusions

Numerical analysis shows that the application of the FO models leads to more than a 50% improvement of the SSE performance index. The commensurate model is worse that the non-commensurate one. This is caused by the evident relation

$$ \min[\mathrm{SSE}(a_0, a_1)] \geq \min[\mathrm{SSE}(a_0, a_1, \nu_1)] \geq \min[\mathrm{SSE}(a_0, a_1, \nu_1, \nu_2)]. \tag{60} $$

The proposed lowering of the total order is of particular importance in the closed-loop systems with multiple inputs and multiple outputs with the same sub-plants.

Acknowledgements. The work was supported by Polish funds of the National Science Center, granted on the basis of decision DEC-2016/23/B/ST7/03686. Partly it was financed by the Lodz University of Technology, Faculty of Electrical, Electronic, Computer and Control Engineering as a part of statutory activity (project no. 501/12-24-1-5418).

REFERENCES

[1] A.A. Kilbas, H.M. Srivastava, and J.J. Trujillo, *Theory and Applications of Fractional Differential Equations*, 523 Elsevier, Amsterdam 2006.

[2] A. Oustaloup, *La dérivation non entière: theéorie, synthèse et applications*, Hermès, Paris 1995.

[3] I. Podlubny, *Fractional Differential Equations*, Academic Press, London 1999.

[4] S.G. Samko, A.A. Kilbas, and O.I. Marichev, *Fractional Integrals and Derivatives*, Gordon and Breach Science Publishers, London 1993.

[5] R. Caponetto, G. Dongola, L. Fortuna, and I. Petras, *Fractional Order Systems: Modeling and Control Applications*, 175 World Scientific Series on Nonlinear Science: Series, vol. 72, Singapore, 2010.

[6] S. Das, *Functional Fractional Calculus for System Identification and Controls*, 239 Springer-Verlag, Berlin-Heidelberg, 2009.

[7] S. Guermah, S. Djennoune, and M. Bettayeb, "Discrete-Time Fractional-Order Systems: Modeling and Stability Issues", *Advances in Discrete Time Systems*, pp. 183–212, 2010.

[8] M.D. Ortigueira, *Fractional Calculus for Scientists and Engineers*, 239. Springer Science + Business Media B.V., Dodrecht Heidelberg London New York 2011.

[9] J. Sabatier, O.P. Agrawal, and T.A. Machado, *Advances in Fractional Calculus. Theoretical Developments and Applications in Physics and Engineering*, Springer Verlag, Dordrecht 2007.

[10] P. Ostalczyk, *Discrete Fractional-Calculus*, World-Scientific, Singapore 2016.

[11] C.A. Vinagre, T.A. Monje, and A.J. Caldero, *Fractional order systems and fractional order actions*, Tutorial Workshop#2: Fractional Calculus Applications in Automatic Control and Robotics. 41st IEEE CDC 2002, pp. 2550–2554.

[12] M. Wyrwas and D. Mozyrska, *On Mittag–Leffler STABIlity of Fractional Order Difference Systems*, Lecture Notes in Electrical Engineering: Advances in the Theory and Applications of Non-integer Order Systems, Ed. Latawiec K.J. and Łukaniszyn M. and Stanisławski R., Springer, 2014, pp. 191-197.

[13] L. Ljung, *System Identification. Theory for the User*, Prentice Hall Ptr, Upper Saddle River 1999.

[14] M. Axtell and E.M. Bise, "Fractional calculus applications in control systems", *Proc. of the IEEE 1990 International Aerospace and Electronics Conference* 2, 563–566 (1990).

[15] R.S. Bressan and B. Piccoli, "Introduction to the Mathematical Theory of Control", *AIMS Series on Applied Mathematics* 2, p. 312 (2007).

[16] C.A. Monje, Y. Chen, B.M. Vinagre, D. Xue, and V. Feliu, *Fractional-order Systems and Controls. Fundamentals and Applications (Advances in Industrial Control)*, 415, Springer-Verlag, London 2010.

[17] D. Valério and J. da Costa, *Fractional Processes and Fractional – An Introduction to Fractional Control*, The Institution of Engineering and Technology, London 2013.

[18] R.S. Barbosa, T.A. Machado, and I.S. Jesus, "Effect of fractional orders in the velocity control of a servo system", *Computers and Mathematics with Applications* 59, 1679–1686 (2010).

[19] F.M. Atıcı and P.W. Eloe, "A transform method in discrete fractional calculus", *International Journal of Difference Equations* 2, 165–176 (2007).

[20] I. Petráš, "Stability of fractional-order systems with rational orders: A survey", *Fractional Calculus & Applied Analysis* 12, 269–298 (2002).

[21] H. Sheng, Y. Chen, and T. Qiu, *Fractional Processes and Fractional – Order Signal Processing: Techniques and Applications, Signals and Communication Technology*, Springer-Verlag, London 2012.